Chapter 8

Single-Phase Motors for Household Applications

Damiano D'Aguanno, Fabrizio Marignetti and Francesco Faginoli

Additional information is available at the end of the chapter

http://dx.doi.org/10.5772/intechopen.79203

Abstract

Single-phase motors are widely used in household applications. Shaded-pole and split-phase capacitor-start single-phase induction motors are very popular for their ruggedness and their comparatively low cost. Recently, line-start single-phase motors are gaining market shares. However, their superior efficiency and torque density are counterbalanced by the higher cost of the rotor construction due to the magnets. This chapter compares the main structures of single-phase line-start motors, presenting their lumped parameter models and the finite element analysis. The equivalent circuits of the single-phase induction motor and of the line-start permanent magnet are derived. Different rotor structures for single-phase line-start permanent magnet (PM) motors are compared. The finite element method (FEM) is used to compare the characteristics of the motors. Motors with the same stator have been tested. No-load and load tests have been performed and compared to the FEM simulations and to the analytical model. Finally, the performances of line-start PM motors are compared to the shaded-pole induction motors in terms of torque density and efficiency.

Keywords: single-phase line-start permanent magnet motors, shaded-pole induction motor, performance analysis, permanent magnets, energy efficiency

1. Introduction

Energy saving is an important aspect of sustainable development in modern society. In this field, electrical machines play a fundamental role in industrial, commercial and residential applications. It is well known that the energy consumed by electrical machines represents the largest part of the total consumption of electricity in the industrial sector. Higher efficiency can lead to the significant reduction of fossil fuel consumption and also of the environmental impact of human activities. For this reason, nowadays and worldwide, all products for industry or residential applications are classified on the basis of their energy efficiency.

Single-phase induction motors are used in household applications due to their robust and simple construction and to their capability for being attached directly to the single-phase grid without using power converters [1, 2]. Split-phase and shaded-pole single-phase induction motors (SPIM) represent today the most common single-phase general purpose motors. As SPIM are inherently not self-starting when directly connected to the grid, they use an auxiliary winding to improve the starting capability. The most significant characteristics of the SPIM are as follows: robust and relatively cheap construction and capability to withstand large overloads. In comparison with three-phase induction motors [3] and to other machine types, SPIMs have a much lower efficiency due to their higher copper and core losses [4].

The motors used in domestic appliances often have a small-rated power, less than 2 kW and run at a constant speed [5].

In this power range, the smaller the motor, the lower the efficiency of the machine. This is mainly due to the fact that both the iron loss and the copper loss are significant in comparison with the rated power. In fact, the stator core of small motors is generally not annealed; the air-gap length is relatively large and the resistance of the stator windings is comparatively large.

Permanent magnet synchronous motors (PMSMs) provide higher efficiency and high-torque density, although they need an inverter for normal operation [6]. Due to dramatic improvements in the magnetic and thermal properties of permanent magnet (PM), materials over the past 40 years, alongside with considerable cost reduction, PM synchronous motors have gained popularity both in the inverter-fed and in the line-start categories [7, 8].

Due to their simple structure and direct connection to the grid, single-phase line-start PM motors (SPLSPMM) represent a good alternative to the induction motor as they produce significant energy savings in the long term. SPLSPMMs are structurally similar to single-phase induction motors with the addition of permanent magnets glued or embedded in the rotor. Line-start PM motors have higher efficiency than SPIMs and operate at near unity power factor [9]. Also, they can be supplied by a three-phase supply source and may be provided with a rotor cage [10, 11]. This motor type is suitable for use in devices such as drain pumps and electric fans [12]. Line-start PM motors start like induction motors and run synchronously like any other type of synchronous motor.

Compared to the widespread induction motors, PM motors with direct online starting ability have higher efficiency, high power factor, low sensitivity towards voltage variations and compact size. They also have the additional advantage of achieving higher power density, besides the capacity to operate at synchronous speed [13, 14].

In particular, the SPLSPMM can be used instead of conventional induction motors for applications like pumps, air conditioners and fans [15]. However, the PM synchronous motor working at line frequency has a major drawback during the starting transient as the stator iron bore must be accurately profiled to increase the starting torque and improve the ability to synchronise with a load attached to its shaft.

During motor start-up, the acceleration torque of the SPLSPMM motor is the average cage torque (if the cage is present) minus the load torque. The permanent magnets on the rotor also generate a braking torque which decreases the starting torque and reduces the ability of the rotor to synchronise. The optimisation of the design of these motors improves the output torque as well as their overall efficiency.

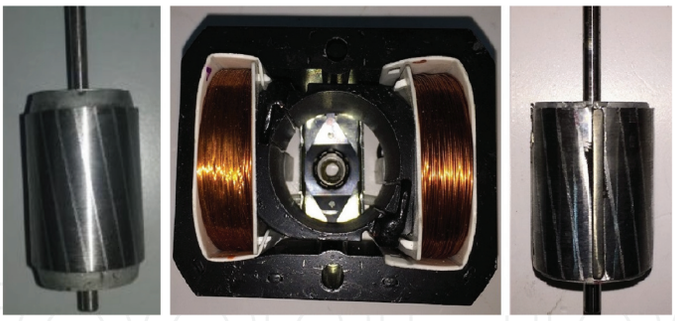

Figure 1. Line-start prototype rotor (right), stator (centre), shaded-pole rotor (left).

The technical literature has dealt with this issue, and different works have investigated how to improve the efficiency of SPLSPMM [16, 17].

Even if the superiority of SPLSPMMs with regard to SPIM is well known, SPIMs are still widely used in many different home appliances.

This chapter analyses the main structures of single-phase motors and compares different rotor structures suitable for SPLSPMM, characterised by different magnet arrangements.

One shaded-pole induction motor (as in **Figure 1**) used in home appliances is compared to different structures of low-cost single-phase line-start PM motor (SPLSPMM) [18, 19] to numerically assess its performance improvement.

The lumped parameter models of the single-phase induction motor and of the single-phase line-start PM motor are presented [20, 21] alongside with their equivalent circuits.

The equivalent circuit of the SPLSPMM is very similar to that of the SPIM. Thanks to this, the SPLSPMM can be easily considered as a particular case of a SPIM with the presence of permanent magnets in the rotor; this leads to an easier comparison of their overall performances.

A comparison of the rotor structures is therefore made through FEM analysis. The optimal solution is experimentally tested.

The study aims at numerically assessing the performances of SPLSPMM and its efficiency in comparison with the shaded-pole SPIM with the same volume and weight [22]. The motors compared basically share the same structure.

The comparison is made by using the finite element method (FEM), the analytical model and the experiments.

Section 4 shows the mathematical model of the motor under test and Section 5 shows the design procedure. The results of the experimental comparison are given in Section 6.

2. Efficiency of single-phase motors

Single-phase shaded-pole induction motors are widely used, but their efficiency is low. Their low performances are due to their intrinsic characteristics. The need for sustainability has led to international regulations on energy efficiency. The IEC 60034-30-1 standard, which was published in March 2014 classifies the motors into four levels of energy efficiency (IE1–IE4).

The IEC 60034-30-1 standard applies both to single- and three-phase motors. The classification is different for motors with different number of pole pairs. The European Union has transposed the IEC 60034-30-1 standard, introducing a timeline for energy efficiency of all motors produced in the power range 0.75–375 kW. Since 2017, all the manufactured electric motors must have efficiency at least equal to the IE3 class (or IE2 if the motor is supplied by an inverter). It is expected that the range is extended in the future. Optimising the motors of everyday use could save huge quantities of energy and keep the competitiveness of industries.

In the literature, many studies are aimed at improving the output characteristics of induction motors [23, 24]. Single-phase line-start induction motors are of two main types:

- split-phase induction motors;
- shaded-pole induction motors.

The first use an auxiliary wining provided with an external impedance. The value of the impedance is chosen by taking different aspects into consideration:

- *Reverse field cancellation*: A capacitor is chosen in order to cancel, as far as possible, the inverse torque present in the machine, to obtain a circular field at the air gap and eliminate the alternative torques with double pulsation with respect to the supply. This technique, however, allows to optimise the performances at one operating speed;
- *Minimisation of the reverse torque/direct torque ratio*: The external impedance is chosen to maximise the performance in a wide speed range;
- *Maximisation of electromagnetic torque*.
- *Maximisation of the torque/current consumption ratio*;

To achieve the same objectives, the shaded-pole induction motors use an auxiliary winding which is generally short-circuited and spatially lagging from the main winding. The impedance of the auxiliary winding introduces the necessary time-lag.

3. Line-start permanent magnet motors

Line-start permanent magnet synchronous motors are structurally similar to single-phase induction motors, except for the permanent magnets located on the rotor. The efficiency of SPLSPMM is higher in comparison to conventional SPIM, and furthermore, they can operate with a close to unity power factor. SPLSPMM are mainly used for household applications, such as refrigerators, compressors or extractor hoods/fans. However, these advantages lead to an increase in production costs. As the cost of high-energy permanent magnets is decreasing, it is possible to expect SPLSPMM gained a wider share of the market, to meet the regulations on energy efficiency.

SPLSPMM combine the advantages of permanent magnet motors to those of the cage rotor. The squirrel cage provides the asynchronous start capability, while the action of the magnets disturbs the transient phase. Another advantage of cage-rotor SPLSPMM is that they can be attached directly to the grid.

At steady state, the motor operates at synchronous speed. At synchronous speed, the currents can be reduced. In fact, in an induction machine, the torque is obtained at the price of the speed difference between the main flux and the rotor. This phenomenon generates Joule losses in the rotor bars and to a lesser extent rotor core loss. Furthermore, the magnetising current required to generate the magnetic field, determines additional losses in the stator. In synchronous machines, the magnetic field is produced by the armature winding and by the excitation, with the majority of the magnetic flux produced by the excitation, while a smaller amount of the reactive power is absorbed by the grid during operation. Moreover, in the case, the excitation field is obtained using permanent magnets; there are no copper losses in the rotor and virtually no core loss.

The main limitations of line-start machines (similar to those of SPIM) are that the air-gap field is elliptic and the starting capabilities are limited. Fortunately, the most limitations can be solved by suitably shaping the magnetic circuit.

The mathematical models of the SPIM and of the SPLSPMM are based on the decomposition of the main fluxes into *direct* and *quadrature* components [25–28].

In this chapter, the mathematical model of the shaded-pole induction machine and of the line-start permanent magnet single-phase machine is presented. The performances of both motor types are compared. The model uses the space vectors [23] to describe the distribution of the induction in the air gap.

3.1. The equivalent circuit of the single-phase induction motor

Single-phase induction motors are widely used in low-power applications (up to a few kW). The construction of these machines is similar to the three-phase version, with one single-phase stator winding and one rotor cage. However, they achieve a lower power density. The stator winding, which generally occupies the two-thirds of the stator periphery is supplied with a sinusoidal voltage, which causes a sinusoidal MMF, too. The magnetic field distribution in the air gap has a fixed position while its amplitude varies sinusoidally as the current.

3.1.1. MMF and torque generated by the main winding

The air-gap magnetic field generated by a single-phase winding is:

$$B(\alpha, t) = B_M(t)\, cos(p\alpha) \tag{1}$$

where p is the number of pole pairs, and α is the angular coordinate in the stator reference.

If in Eq. 1 is set:

$$B_M(t) = N\xi \frac{4}{\pi} \frac{1}{2p\delta} \mu_o\, i(t) \tag{2}$$

with N number of turns per pole pair; ξ the winding factor; δ the width of the air gap; μo the permeability of vacuum.

Considering the case of a sinusoidal supply:

$$i(t) = I_M\, cos(\omega t) \tag{3}$$

Using Eq. (1), one has:

$$B(\alpha, t) = k\, I_M\, cos(\omega t)\, cos(p\alpha) \tag{4}$$

which represents an electromagnetic wave varying its amplitude with time. Eq. (4) can be easily rewritten by using trigonometric assumptions:

$$B(\alpha, t) = \frac{k\, I_M}{2} [cos(\omega t + p\alpha) + cos(\omega t - p\alpha)] \tag{5}$$

This means that the magnetic field of a single-phase winding can be achieved as the sum of two different fields with the same amplitude and with different verse of rotation (**Figure 2**).

These two fields produce the same effect on the rotor. The field rotating in the same direction as the rotor is called *direct field* while the other *reverse field*. Similarly, the electromechanical torque (T) can be considered as the sum of the direct torque T_d, caused by the direct field and of the reverse torque T_i, caused by the reverse field. Obviously, the values of these torques depend on the speed of the rotor. T_d and T_i are equal if the speed is zero, that is, the slip is equal to one (because at zero slip the magnetic fields having equal amplitudes, rotate with same speed but opposite directions). In all other operating points the values of torque are different.

Hence, two slips can be defined, one direct and one reverse:

$$s_d = \frac{n_o - n}{n_o} \tag{6}$$

$$s_i = \frac{n_o + n}{n_o} \tag{7}$$

In order to study the SPIM, a simplification can be introduced by considering the motor as the union of two three-phase machines. The system can be studied with the technique of the superposition of the effects.

The main drawback of the pure single-phase induction machine is that is not self-starting, because at the starting point the resulting torque is null. When the rotor rotates, a non-zero net torque arises.

3.1.2. Reverse field cancellation

In order to solve the problem of cancelling the reverse field produced by the primary winding of the single-phase induction motor, different techniques can be applied. Generally, this is done by adding

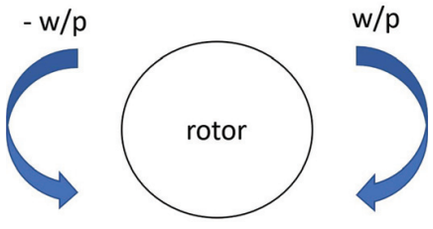

Figure 2. Field rotation directions.

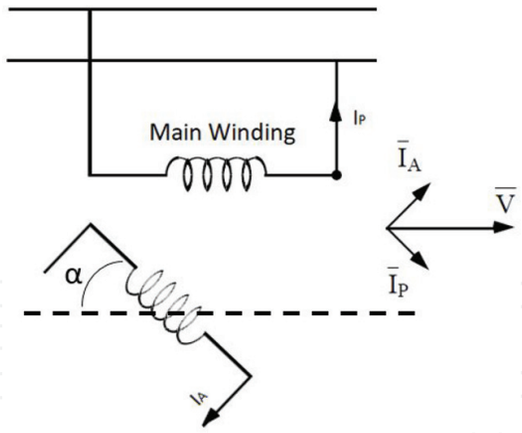

Figure 3. Simplified circuit diagram of a split-phase induction motor.

an auxiliary winding with a magnetic axis displaced γ electric radians from the main winding and supplying the two windings with currents mutually displaced in time of an angle φ (**Figure 3**).

The auxiliary winding produces the additional field *Ba*:

$$B_a(\alpha, t) = B_{aM}(t)\, cos(p\alpha + \gamma) \tag{8}$$

If γ is positive, then the auxiliary winding is lagging. If the auxiliary winding is supplied with a current lagging φ behind the current in the main winding in Eq. 5, the flux density distribution becomes:

$$\begin{aligned} B_a(\alpha, t) &= k_a I_{aM} cos(\omega t - \varphi) cos(p\alpha + \gamma) = \\ &= \frac{k_a I_{aM}}{2} \cdot [cos(\omega t - p\alpha - \gamma - \varphi) + cos(\omega t + p\alpha + \gamma - \varphi)] \end{aligned} \tag{9}$$

The resultant flux density in the air gap is achieved summing Eq. (9) to Eq. (5) and consists of two rotating fields, one in the *direct direction*:

$$B_d = \frac{k\, I_M}{2}\, cos(\omega t - p\alpha) + \frac{k_a\, I_{aM}}{2}\, cos(\omega t - p\alpha - \gamma - \varphi) \tag{10}$$

and the other one in the *reverse direction*:

$$B_r = \frac{k\, I_M}{2}\, cos(\omega t + p\alpha) + \frac{k_a\, I_{aM}}{2}\, cos(\omega t + p\alpha + \gamma - \varphi) \tag{11}$$

To ideally cancel the reverse field, two conditions must be considered:

1. The MMF amplitudes of the primary and auxiliary fields must be equal:

$$k_a \cdot I_{aM} = k \cdot I_M,$$

2. The following relationship between the geometrical and the time phase lags must hold:

$$\gamma - \varphi = \pi,$$

Finally, the maximum direct field amplitude is achieved if:

$$\gamma = -\varphi. \tag{12}$$

In the case, the two conditions for reverse flux cancellation are achieved, the resultant flux density in the air gap is achieved by summing Eq. (9) to Eq. (5):

$$B(\alpha, t) = k\, I_M\, [cos(\omega t - p\alpha) + cos(\omega t - p\alpha - \gamma - \varphi)] \tag{13}$$

Eq. (13) represents one field rotating in one direction, like in a three-phase machine. Obviously, the perfect cancellation may be achieved only at one working point, for example, at start-up or at nominal load.

In split-phase machines, condition 2 is achieved by displacing the auxiliary winding of $\gamma = \pi/2$ that means $\varphi = -\pi/2$. The minus sign means that the auxiliary current *leads* the main current.

Therefore, the split-phase SPIM includes two stator windings: one *main winding* and one *auxiliary winding*, displaced of 90°. If the auxiliary winding is used for starting, it can be excluded when the machine reaches a fixed operating condition.

The current lag of $\pi/2$ is produced by introducing a capacitor in series to the auxiliary winding. This is necessary to provide the self-starting capability and to improve its performance, so that the phase displacement between the currents circulating in the two stator windings, creates an imbalance between the direct torque and the reverse torque. This phase shift is possible because the ohmic-capacitive nature of one of the winding (due to the presence of the capacitor).

Since the auxiliary winding can be disconnected over a fixed speed, capacitor-start induction machine can be divided into permanent capacitor topology (**Figure 4**) and starter capacitor topology (**Figure 5**).

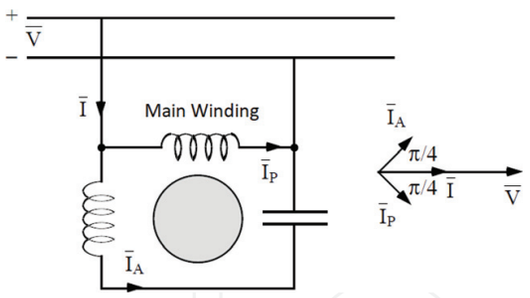

Figure 4. Permanent capacitor induction motor.

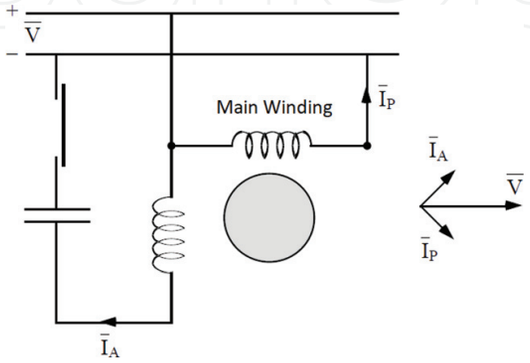

Figure 5. Capacitor-start single-phase induction motor.

For the capacitor-start motor, the value of the capacity is selected to achieve the desired starting performance, while for the permanent capacitor motors, it is generally the result of a trade-off between performances under different load conditions.

In shaded-pole SPIMS, the auxiliary winding is, instead, composed of two short-circuited windings wound around the pole shoes. The angle ψ is varied by varying the number of the short-circuited turns until the desired performance is reached.

3.2. Analysis of the single-phase induction motor

Based on the air-gap flux density distribution in Section 3.1.2, it is possible to compute the EMF induced in the stator and rotor windings. Afterwards, the electromagnetic torque is obtained and finally the equivalent circuit is derived.

3.2.1. Resultant air-gap flux density

The air-gap flux density is the sum of the flux density distribution of the stator windings and of the cage:

$$B(\alpha, t) = B_{stator} + B_{cage} \tag{14}$$

where B_{stator} and B_{cage} can be derived from Eqs. (10) and (11):

$$\begin{aligned} B_{stator} &= \sqrt{2}\,\frac{\mu_0}{\pi p}\,N_i \xi_i\, Re[I_{fs} e^{j(\omega t - p\alpha)} + I_{bs} e^{j(\omega t + p\alpha)}] \\ B_{cage} &= \sqrt{2}\,\frac{\mu_0}{2\pi p \delta}\, Re[I_{fr} e^{j(\omega t - p\alpha)} + I_{br} e^{j(\omega t + p\alpha)}] \end{aligned} \tag{15}$$

where I_{fs} and I_{fr} are the direct and the reverse component of the stator currents system, respectively. If the cancellation of the reverse flux is not perfect, the amplitudes of these current components are different. The same is for the cage.

At sinusoidal steady state, the main harmonic of the air-gap flux density is:

$$\begin{aligned} &B(\alpha, t) = \sqrt{2}\,\frac{\mu_0}{\pi \delta}\, N_i \xi_i\, Re[(I_{fs} + \kappa I_{fr}) e^{j(\omega t - p\alpha)} + (I_{bs} + \kappa I_{br}) e^{j(\omega t + p\alpha)}] \\ &\text{with} \quad \kappa = \tfrac{1}{2pN_i\xi_i} \end{aligned} \tag{16}$$

3.2.2. Stator back EMFs

The EMF of one stator winding can be obtained by summing the EMF of each coil.

$$e_{is} = -\frac{1}{2}\, pDl \sum_{\nu=0}^{q_i - 1} z_{\nu i}\, \frac{d}{dt} \int_{-\frac{\pi}{2p} - \frac{\pi(q_1-1)}{Q} + \frac{2\pi\nu}{Q} + \frac{\alpha_i}{p}}^{\frac{\pi}{2p} + \frac{\pi(q_1-1)}{Q} + \frac{2\pi\nu}{Q} + \frac{\alpha_i}{p}} B(\alpha, t)\, d\alpha \tag{17}$$

where D is the diameter of the machine; z_{vi} is the number of conductors in slot.

The EMF induced in the stator windings can be evaluated as:

$$e_{is} = -\sqrt{2} X_m \beta_i \, Re[j(I_f e^{-j(\alpha_i - \alpha_1^*)} + I_b e^{-j(\alpha_i - \alpha_1^*)}) \, e^{j\omega t}] \tag{18}$$

where the following equation was assumed:

$$X_m = \frac{\mu_0}{\pi \delta} \omega D l (N_i \xi_i)^2$$

3.3. Rotor back EMFs

The EMFs in the rotor bars are obtained in the same way as before.

$$e_{kr} = -\frac{1}{4} Dl \frac{d}{dt} \int_{-\frac{\pi}{2p} + \omega_r t + \frac{2\pi(k-1)}{m_r}}^{\frac{\pi}{2p} + \omega_r t + \frac{2\pi(k-1)}{m_r}} B(\alpha, t) \, d\alpha \tag{19}$$

The EMF induced in each rotor bar is the sum of two sinusoidal components with pulsation $(\omega + p_{\omega r})$ e $(\omega - p_{\omega r})$:

$$e_{kr} = -\sqrt{2} \frac{\mu_0}{2\pi p \delta} Dl N_i \xi_i \, Re[j(I_f \, (\omega - p\omega_r) \, e^{-j(\omega - p\omega_r)t} \, e^{j\frac{2\pi p(k-1)}{m_r}} + \\ + I_b \, (\omega + p\omega_r) \, e^{j(\omega + p\omega_r)t} \, e^{j\frac{2\pi p(k-1)}{m_r}}] \tag{20}$$

3.4. Electromagnetic torque expression

The electromechanical torque can be evaluated as:

$$T = -\frac{D^2 l}{4} \int_0^{2\pi} B(\alpha, t) \, \Theta_r(\alpha, t) \, d\alpha \tag{21}$$

with $B(\alpha, t)$ the distribution of the induction in the air gap and $\Theta_r(\alpha, t)$ the rotor current density:

$$\Theta_r(\alpha, t) = \frac{2}{D} \frac{d}{d\alpha} [\Delta F_r(\alpha, t)] \tag{22}$$

where $\Delta F_r(\alpha, t)$ is the MMF caused only by the rotor currents:

$$\Delta F_r(\alpha, t) = \frac{\delta}{\mu_0} B(\alpha, t) = \frac{\delta}{\mu_0} (\sqrt{2} \frac{\mu_0}{2\pi p \delta} Re[\frac{I_{fr}}{\rho} e^{j(\omega t - p\alpha)} + \frac{I_{br}}{\rho} e^{j(\omega t + p\alpha)}]) \tag{23}$$

Eq. 22 becomes:

$$\Theta_r(\alpha, t) = \frac{2\sqrt{2} N_i \xi_i p}{D\pi} Re[-jI'_{fr} \, e^{j(\omega t - p\alpha)} + jI'_{br} \, e^{j(\omega t + p\alpha)}] \tag{24}$$

By substituting Eq. 24 and Eq. 16 in Eq. 21 and finally solving, the expression of the electromagnetic torque is obtained:

$$T = -X_m \frac{p}{\omega} Re[jI_f I'_{fr} - jI_b I'_{br} + j(I_f I'_{br} - I_b I'_{fr}) \, e^{j2\omega t}] \tag{25}$$

where the following equation was assumed: $I_f = I_{fs} + \rho I_{fr}$ and $I_b = I_{bs} + \rho I_{br}$.

Therefore, the electromagnetic torque in a single-phase induction motor is the sum of three terms:

1. Direct electromagnetic torque:

$$T_d = -X_m \frac{p}{\omega} Re[jI_f I_{fs}]$$

2. Reverse electromagnetic torque:

$$T_i = -X_m \frac{p}{\omega} Re[-jI_b I_{bs}]$$

3. Electromagnetic torque with pulsation 2ω:

$$T_a = -X_m \frac{p}{\omega} Re[j(I_f I_{bs} - I_b I_{fs})\, e^{j2\omega t}]$$

3.5. Mathematical model

The mathematical model of the SPIM is obtained by considering the fundamental harmonic of the air-gap flux density distribution.

The impedances of the two circuits (**Figure 6**), including the external impedance are: $Z_1 = R_1 + jX_1$ and $Z_{t2} = R_2 + R_c + j(X_2 + X_c)$.

The currents I_1 and I_2 can be expressed as a function the direct and reverse components of the stator currents:

$$\underline{I}_1 = \frac{\underline{I}_{fs} + \underline{I}_{bs}}{2} \tag{26}$$

$$\underline{I}_2 = \frac{\underline{I}_{fs} + \underline{I}_{bs}}{2j\beta} \qquad \beta = \frac{N_2 \xi_2}{N_1 \xi_1} \tag{27}$$

The equations referred to the various nets of the equivalent circuits are:

where

$$\begin{aligned} +\underline{V} &= \dot{A}\underline{I}_{fs} + \dot{B}\underline{I}_{bs} \\ \pm\underline{V} &= \dot{C}\underline{I}_{fs} + \dot{D}\underline{I}_{bs} \end{aligned} \tag{28}$$

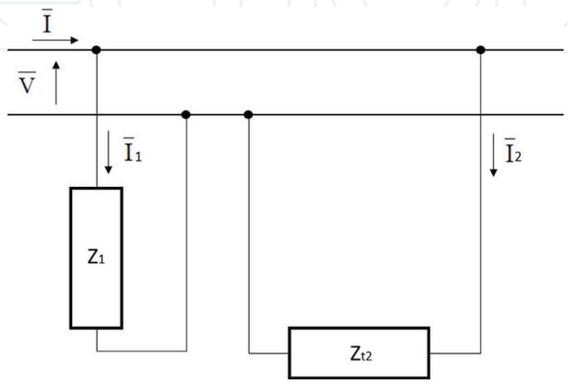

Figure 6. Grid connection of a capacitor-start single-phase induction motor.

where

$$\dot{A} = \frac{(R_1 + jX_1)}{2} + jX_m \cdot [1 - \frac{jX_m}{\frac{R'_r}{s} + jX_t}]$$

$$\dot{B} = \frac{(R_1 + jX_1)}{2} + jX_m \cdot [1 - \frac{jX_m}{\frac{R'_r}{2-s} + jX_t}]$$

$$\dot{C} = \frac{[R_2 + R_c + j(X_2 + X_c)]}{2j\beta} + \beta X_m [1 - \frac{jX_m}{\frac{R'_r}{s} + jX_t}]$$

$$\dot{D} = -\frac{[R_2 + R_c + j(X_2 + X_c)]}{2j\beta} + \beta X_m [1 - \frac{jX_m}{\frac{R'_r}{2-s} + jX_t}]$$

The expression of the electromagnetic torque is finally recalled.

$$T_m = -\frac{p}{\omega} X_m^2 [\frac{\frac{R'_r}{s}}{(\frac{R'_r}{s})^2 + j(X_m + X'_r)^2} I_{fs}^2 - \frac{\frac{R'_r}{2-s}}{(\frac{R'_r}{2-s})^2 + j(X_m + X'_r)^2} I_{bs}^2] \tag{29}$$

3.6. The equivalent circuit of the single-phase induction motor

The equations, which define the mathematical model of the single-phase induction motor with an auxiliary winding and external impedance, can be graphically translated into equivalent circuits.

Referring to the model Eqs. (28) after some manipulations, one can write:

$$\begin{aligned} \underline{V}\frac{\beta \pm j}{\beta} &= [\frac{\dot{Z}_2 + \dot{Z}_c}{2\beta^2} + jX_m(1 - \frac{jX_m}{\frac{R'_r}{s} + jX_t})]I_{fs} + (I_{fs} + I_{bs})\frac{[\dot{Z}_1 - \frac{Z_2 + Z_c}{\beta^2}]}{4} \\ \underline{V}\frac{\beta + j}{\beta} &= [\frac{\dot{Z}_2 + \dot{Z}_c}{2\beta^2} + jX_m(1 - \frac{jX_m}{\frac{R'_r}{2-s} + jX_t})]I_{bs} + (I_{fs} + I_{bs})\frac{[\dot{Z}_1 - \frac{Z_2 + Z_c}{\beta^2}]}{4} \end{aligned} \tag{30}$$

4. The line-start permanent magnet synchronous motor

The model of the line-start PM machine is derived hereafter on the basis of the model of the shaded-pole machine without any auxiliary winding.

4.1. Stator winding flux density distribution in the air gap

In a single-phase machine with p pole pairs, the magnetic field in the air gap is fixed in space and variable in time due to the structure of the motor and its winding. The armature winding is therefore unable to create a rotating field in time and space. The first harmonic of the stator magnetic field can be written as:

$$B_s(\alpha, t) = K\, i_s(t) \cdot cos(p\alpha) \tag{31}$$

where K is

$$\mu_0\, f\, \frac{N\, K_w}{2\delta}. \tag{32}$$

with f form factor, which is

$$f = \frac{4}{\pi} \tag{33}$$

in the case of rectangular magnetomotive force (MMF). The equation of the stator winding flux density is:

$$B_s = \sqrt{2}\frac{\mu_0}{\pi p} N K_w Re\left[I_{fs} e^{j(\omega t - p\alpha)} + I_{bs} e^{j(\omega t + p\alpha)}\right] \tag{34}$$

This field can be divided into two components, namely, the direct and the reverse field.

4.2. Total air-gap flux density of SPLSPMMs

The air-gap flux density of line-start single-phase PM synchronous motors is the sum of two contributions: the stator winding flux density and the permanent magnet flux density distribution B_{pm}. In some cases, an incomplete squirrel cage may be added to improve the starting performance and a further flux density distribution B_c is added:

$$B_p\ (\alpha, t) = B_s + B_c + B_{pm} \tag{35}$$

with:

$$B_s = \sqrt{2}\frac{\mu_0}{\pi p} N_i \xi_i Re[I_{fs} e^{j(\omega t - p\alpha)} + I_{bs} e^{j(\omega t + p\alpha)}] \tag{36}$$

$$B_c = \sqrt{2}\frac{\mu_0}{2\pi p\delta} Re[I_{fr} e^{j(\omega t - p\alpha)} + I_{br} e^{j(\omega t + p\alpha)}] \tag{37}$$

$$B_{pm} = B_M cos(p\alpha - \omega_r t + \beta) \tag{38}$$

At sinusoidal steady state and ω_r rotor speed, one has:

$$\begin{aligned} B_{\alpha,t} = {} & \sqrt{2}\frac{\mu_0}{\pi\delta} N_i \xi_i Re[(I_{fs} + \rho I_{fr}) e^{j(\omega t - p\alpha)} + (I_{bs} + \rho I_{br}) e^{j(\omega t + p\alpha)}] \\ & + B_M cos(p\alpha - \omega_r t + \beta) \end{aligned} \tag{39}$$

where I_{fs} and I_{bs} represent the forward and backward components of the stator current. Each flux density component gives rise to a contribution to the back EMF.

The more accurate model of a SPLSPMM is that of Ref. [14], which is based on [1]. The model analyses a SPLSPMM with an asymmetrical stator winding, an auxiliary winding and PMs on the rotor causing braking and pulsating torques. The model is based on a combination of symmetrical components and d-q axis theory. For a motor without an auxiliary winding, the V_q symmetrical component is zero, while $\underline{V_d} = 2V_m$. At synchronous steady state, the forward voltage is synchronised with the rotor, and the model can be simplified using the average of the apparent d-axis impedance, while the q-axis part is unnecessary. The resulting d-axis component model at steady state is represented as the equivalent circuit of **Figure 7** for a SPIM and **Figure 8** for a SPLSPMM.

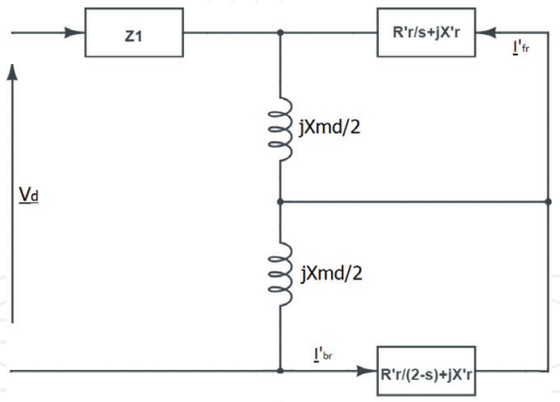

Figure 7. Equivalent circuit of a single-phase induction machine.

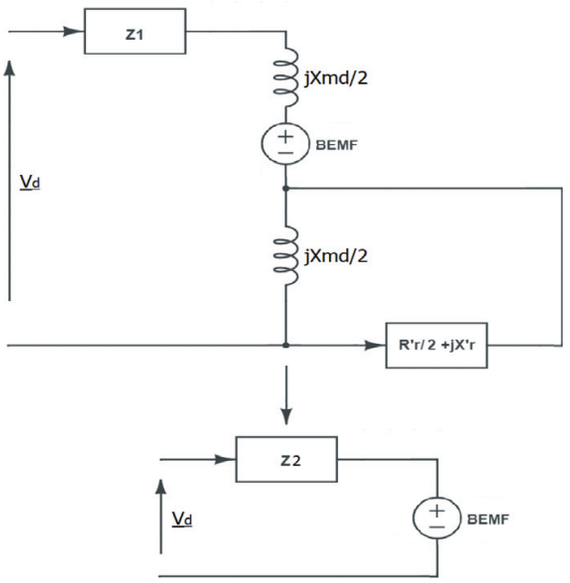

Figure 8. Equivalent circuits of a single-phase SPLSPMM machine, where $Z1$ is the stator impedance; X_{md} is the d-axis magnetisation reactance referred to the stator (main) winding; R_r^l is the rotor resistance referred to the stator winding; X_r^l is the rotor leakage reactance referred to the stator winding; *BEMF* is the equivalent back EMF caused by the presence of the magnets; $Z2$ is the average of the apparent d-axis impedance $Z2 = [Z1 + jX_{md}] + [jXmd//(Rr^l/2 + jXr^l)]$ [14].

5. Selection of the optimum configuration

5.1. Machine specifications and no-load field simulation

Different machine configurations have been numerically compared with the help of the finite element method (FEM). All configurations share the same stator core, which is the same as the core of the SPIM used as a benchmark, while the number, the type and the shape of rotor magnets are different. An incomplete cage is present on the rotor to improve the starting capability of the motor.

Table 1 shows the main dimensions and specifications of the considered motors. The winding is made of 1723 turns with a 0.2 mm copper wire, the material used for the cage is aluminium.

The first configuration is directly derived from the shaded-pole induction motor and includes two surface-mounted NdFeB magnets. The FEM motor model with the flux density contour is shown in **Figure 9(a)**. The volume of the magnets required by this structure is considerable and also the manufacturing cost is larger than that of the following solutions; therefore, it will be included here only for the sake of completeness. The incomplete cage is used to ensure starting in all configurations.

The second configuration is similar to the first, it is made of two NdFeB magnets but instead of being surface mounted they are buried inside the rotor. The FEM motor model with the flux density contour is in **Figure 9(b)**.

The third configuration is based on the second and includes two further inset NdFeB magnets to increase the field in the *d*-axis of the rotor. The FEM motor model with the flux density contour is in **Figure 9(c)**.

In order to further investigate the role of the middle magnets, a fourth configuration is proposed. It is the same as the third, although the two middle magnets are closer to the air gap. The FEM motor model with the flux density contour is in **Figure 9(d)**.

Finally, a low-cost configuration is presented. It is the same as the third configuration; it is equipped with two ceramic middle magnets instead of the inset NdFeB magnets. The FEM motor model with the flux density contour of this configuration is in **Figure 9(e)**.

5.2. Flux linkage

The flux linkage is numerically calculated for each of the above structures. The flux linkages of the different configurations are shown in **Figure 10**.

It can be seen that, while the first configuration produces the highest flux linkage, there is no significant difference among the other configurations. Based on cost considerations, configurations 2 and 4 must be preferred.

The configuration chosen is shown in **Figure 1** and in **Figure 9(b)**, with two Grade 32 NdFeB magnets embedded in the rotor. This configuration offers the maximum flux density with the lowest increase in the cost of manufacturing the machine. Furthermore, this configuration is the easiest to produce.

Element	Dimension
Stator height	67.6 mm
Stator width	84.6 mm
Rotor diameter	34.24 mm
Air gap	0.4 mm
Lamination length	19 mm
Poles	2
Turns	1723

Table 1. Prototypes main dimensions and specifications.

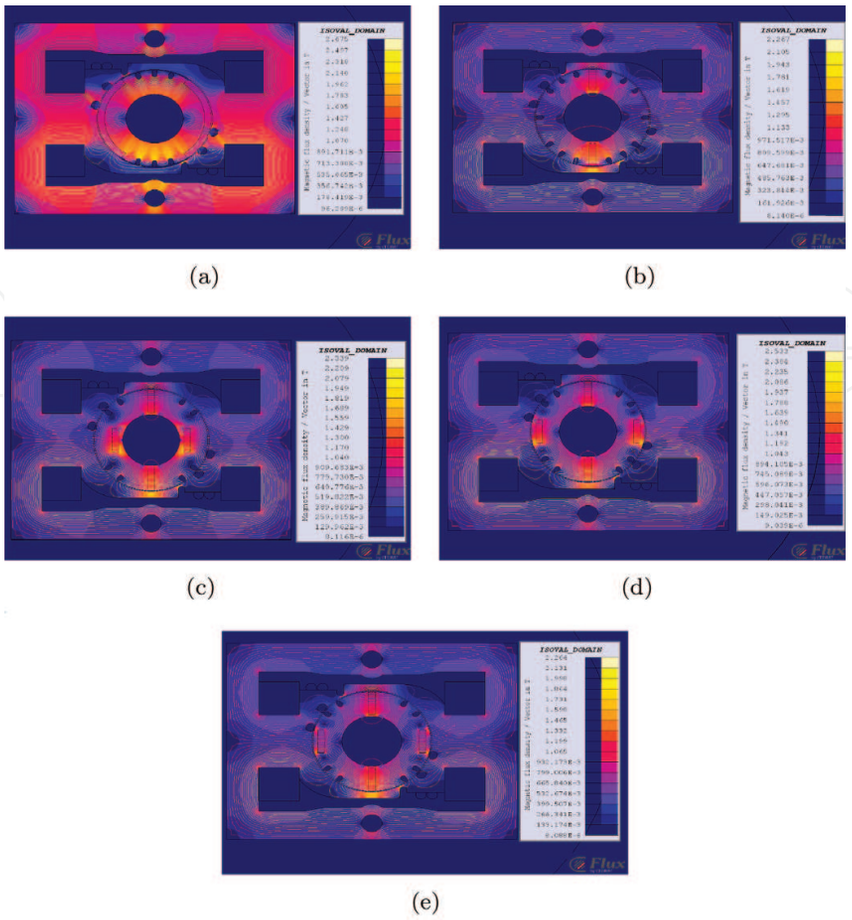

Figure 9. No load FEM simulations. (a) FEM simulation result of the first rotor configuration with two surface NdFeB magnets (model 1). (b) FEM simulation result of the second rotor configuration with two inset NdFeB magnets (model 2). (c) Third rotor configuration with with four NdFeB (position 1) simulation result (model 3). (d) Configuration with four NdFeB magnets (position 2) simulation result (model 4). (e) Configuration with two NdFeB magnets and two ceramic magnets (position 1) simulation result (model 5).

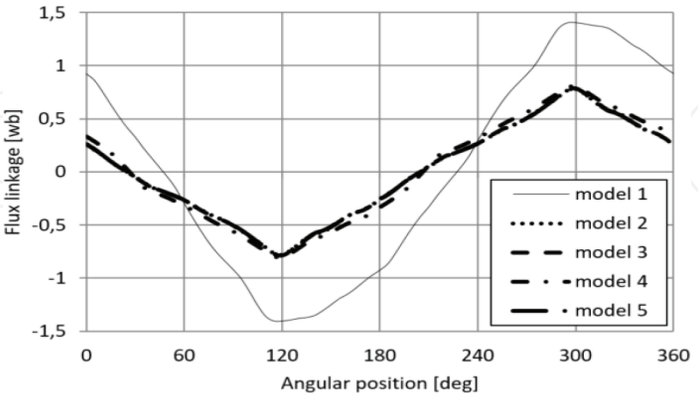

Figure 10. Flux linkages of the different structures for different rotor positions.

The back EMF can be calculated from the flux linkages as:

$$e = \frac{d\phi}{dt}\frac{d\theta}{dt} = \frac{d\phi}{dt}\omega_r \tag{40}$$

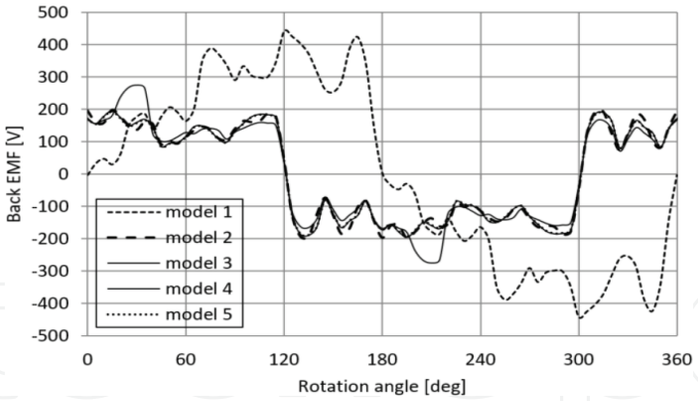

Figure 11. Predicted back EMFs versus rotor position model 1, 2, 3, 4, 5.

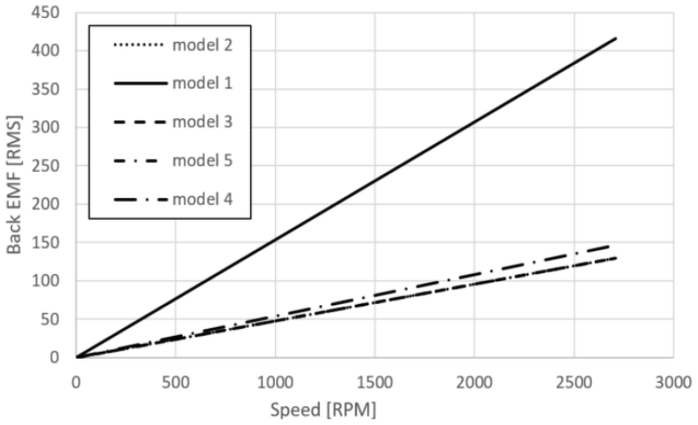

Figure 12. Back EMFs for different rotor speed different solutions.

Using Eq. (40), the back EMF is computed over a complete rotation of the rotor and its RMS value is extracted. On the other hand, the trends for the predicted back EMF are shown in **Figure 11**. The RMS value of the back EMF versus the speed (for the different solutions) is shown in **Figure 12**. One can notice that the trend is, as expected, approximately linear. These values are compared to the experimental results in Section 6 (for the chosen solution).

6. Experimental tests

To compare the SPLSPMM's performances with the SPIM's, the SPLSPMM has been supplied with a single-phase inverter implementing a V/Hz ramp.

6.1. Parameter identification of SPLSPMMs

In order to obtain the machine model parameters and study its performances, both no-load and load tests have been performed. The test bench is shown in **Figure 13**.

The equivalent circuit parameters, derived from tests, are shown in **Table 2**, while **Figure 14** shows the trend of the magnetisation reactance as a function of the voltage (which has been implemented in the mathematical model).

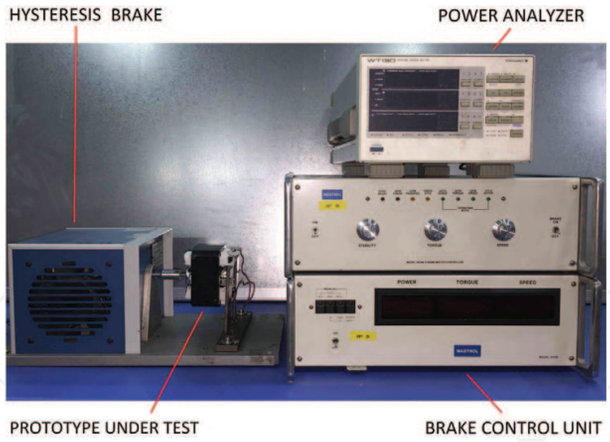

Figure 13. Test bench.

Parameter	Value
Rs	76.37 Ω
Xs	40.21 Ω
R_r^I	10.19 Ω
X_r^I	20.10 Ω
Xmd	113.34 Ω

Table 2. Equivalent circuit parameters.

For the open circuit test, the machine is coupled to an induction machine and the terminals of the motor under test (MUT) are open. The terminal voltages are measured at different values of the speed. The trend of the back EMFs RMS amplitudes is approximately linear as shown in **Figure 15**. From the same figure, it is possible to verify that the analytically predicted trend is very close to the experimental results. The slight differences are caused by the manufacturing process (which may have degraded the magnet superficially) and by the mathematical approximations.

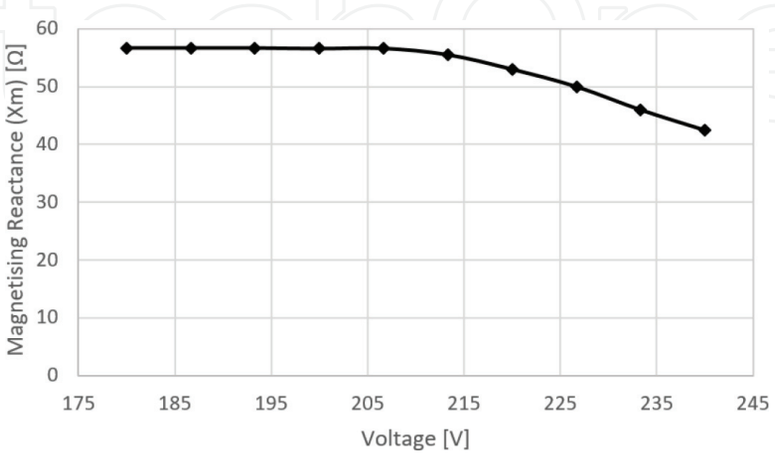

Figure 14. Magnetisation reactance as a function of voltage.

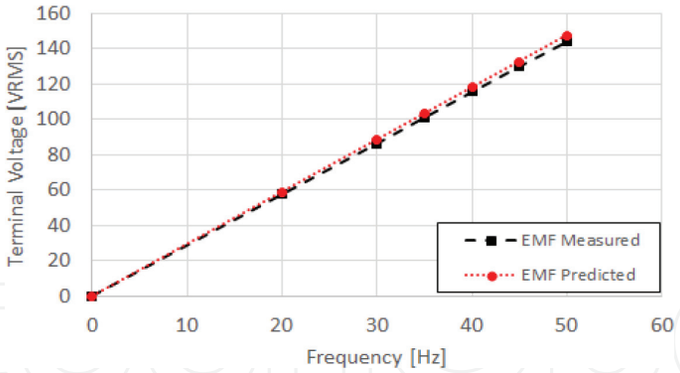

Figure 15. Back EMFs comparison.

The value and waveform shape of the back EMF at 2710 rpm (45.2 Hz) are shown in **Figure 16**. Considering the same operating point, a FEA simulation is performed, and the behaviour of the machine is shown in **Figure 11**.

The predicted and the experimental voltage RMS values are the same and the shapes of the back EMFs are approximately the same, except for the larger ripple presented by the experimental data, which is due to the rotor cage slotting.

In **Table 3**, the rated operating point of the shaded-pole machine is compared with two operating points of the prototype. Considering a fixed frequency of 50 Hz and a variable voltage, the maximum torque is delivered when the motor is supplied with 230 V, while the maximum efficiency is achieved when supplied with 190 V. More results are shown in Section 6.2.

The data shown in **Table 3** demonstrate that only with a slightly different rotor configuration of the machine, the performances improved considerably. This means that the motor can be used both in a completely different field and in similar applications, as in the case we are considering, with significantly better performances.

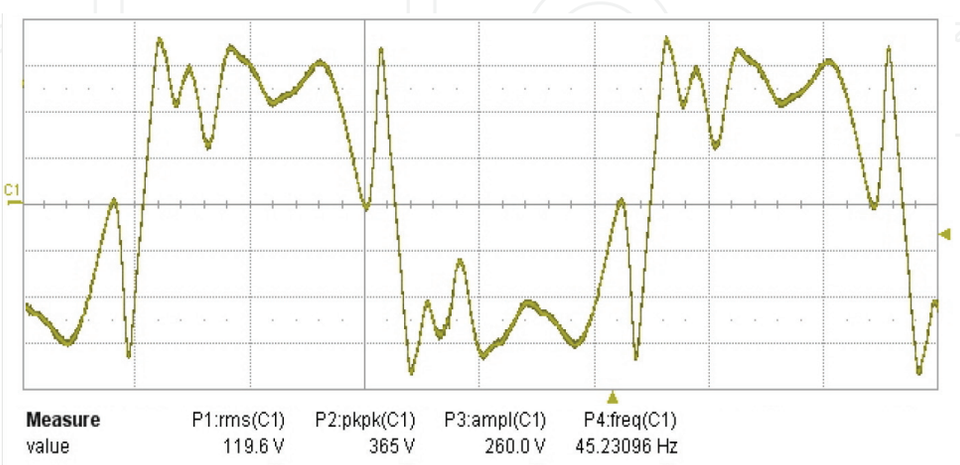

Figure 16. Measured back EMFs versus rotor position.

Quantity	Shaded-pole machine (rated values)	Prototype maximum torque O.P.	Prototype maximum efficiency O.P.
Current [A]	0.214	0.92	0.75
Voltage [V]	230	230	190
Electric power [W]	68	148	123
Rated speed [RPM]	2600	3000	3000
Power [W]	27	76.8	89.6
Rated frequency [Hz]	50	50	50
Efficiency [%]	12.00	62.44	73.59

Table 3. Motors characteristics.

6.2. Characterisation of the SPIM

The SPIM has one stator winding (main winding) and one short-circuited winding, while the rotor is of the squirrel-cage type. The single-phase induction motor without its auxiliary winding is not self-starting. When the motor is connected to a single-phase supply, the main winding carries the alternating current, which produces a pulsating magnetic field. To generate torque, an auxiliary winding is needed.

The SPIM used shares the same magnetic circuit as the SPLSPMM. The induction machine is supplied with its rated voltage and frequency, hence 230 V and 50 Hz, and the load torque is increased with steps between 0 and the maximum torque.

In order to have an idea of the performances of the shaded-pole motor here are some data. The maximum torque achievable by the motor in these conditions is 1.26 kg cm at 2076 rpm. The supply current of the motor is 0.82 A in this operating point. The input power is 107 W and the output power is 27 W, hence the efficiency in this point is 25.23%. The maximum SPIM efficiency of 28.16% is achieved at 2350 rpm, with an input current of 0.78 A and an output torque of 1.14 kg cm. The same test has been performed with different values of supply voltage between 180 V and 240 V. The highest value of torque, in these conditions, is delivered at 240 V and it is 1.23 kg cm, while the highest efficiency of 27.03% is obtained at 210 V.

6.3. Characterisation of the SPLSPMM

The SPLSPMM has been supplied by a single-phase inverter implementing a V/f law. The test has been performed with different values of the supply voltage ranging between 180 and 230 V. The torque trend versus the input current is shown in **Figure 17**. At 230 V and 3000 rpm the achieved torque is 2.91 kg cm with an input current of 0.92 A. The torque has been experimentally evaluated and compared with the analytical torque achieved using the equivalent circuit (**Figure 18**). **Figure 19** shows the trend of the efficiency of the SPLSPMM versus the input current at different voltages and frequencies. The maximum efficiency is 62.44% with 0.75 A, 2.49 kg cm at 3000 rpm. The highest torque value is delivered at 220 V and it is 2.6 kg cm, while the most efficient point is obtained at 190 V with 73.59%.

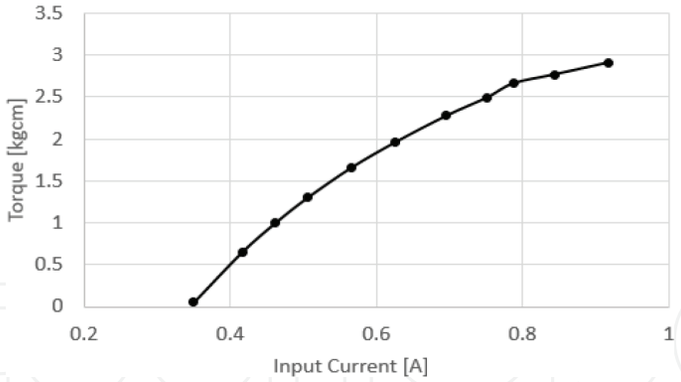

Figure 17. The SPLSPMM's trend of the torque with the input current by *V/f* inverter supply.

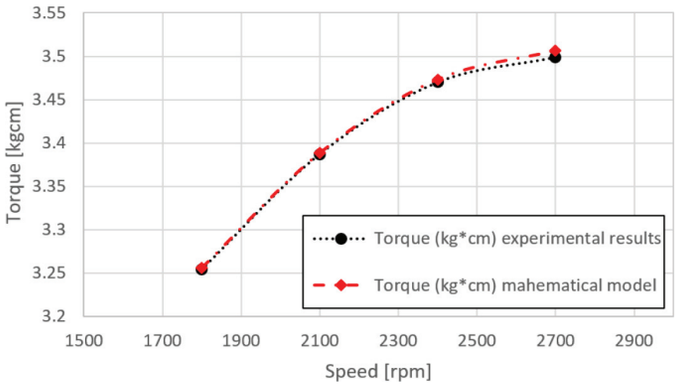

Figure 18. SPLSPMM torque trend comparison between experimental results and mathematical model.

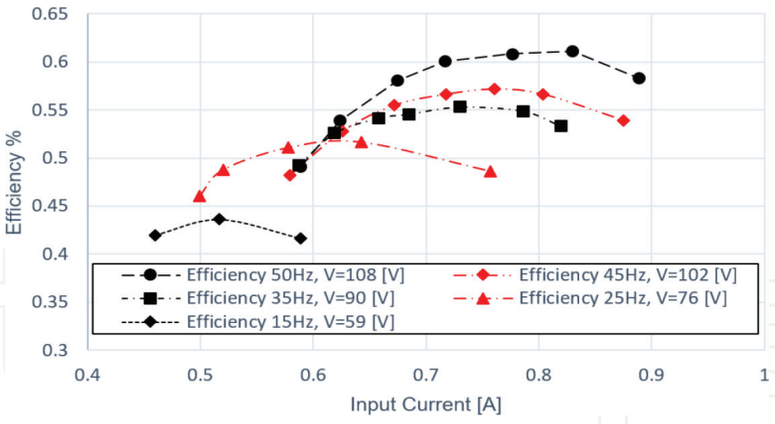

Figure 19. The SPLSPMM's efficiency at different frequencies.

6.4. Comparison between the SPLSPMM and the SPIM

To assess the performances of the two motor types, the SPLSPMM and the SPIM have been tested in the same operating conditions. The performance comparison is made by connecting the two motors to a sinusoidal power supply at 50 Hz frequency and variable voltage. The efficiency characteristic and the torques are compared in **Figures 20** and **21**.

The two figures highlight the supremacy of the SPLSPMM in terms of torque density and efficiency. The superiority is mainly due to the mechanism of torque production of the

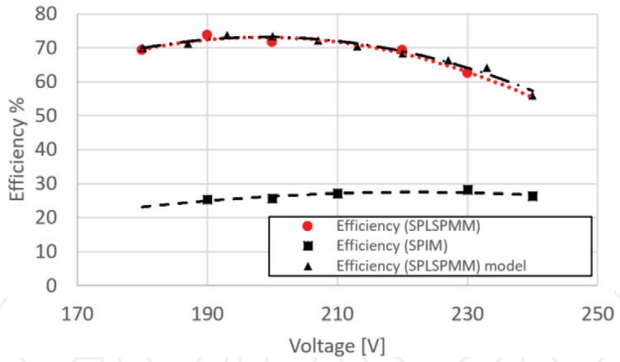

Figure 20. Efficiency comparison.

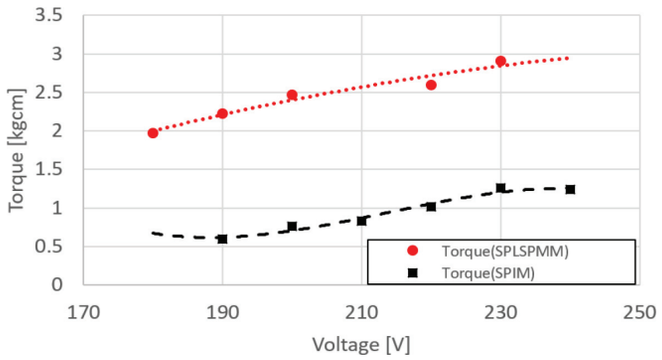

Figure 21. Torque comparison.

SPLSPMM. At fixed torque, the current of the SPLSPMM is lower, reducing the Joule loss in the stator winding. Moreover, the loss component in the rotor cage is reduced and the absence of the auxiliary winding (shaded pole) further reduces the Joule losses. The increase in iron losses due to magnets is not significant. Hence, as was imaginable, thanks to a simple change in the rotor structure, the overall performances get better.

7. Conclusion

This chapter has proposed a mathematical and experimental analysis of a SPLSPMM. Different structures of SPLSPMMs have been simulated with FEM and compared. A prototype has been built, analysed and tested.

Starting from the mathematical model of the single-phase shaded-pole motor, an equivalent circuit has been proposed for the SPLSPMM. The equivalent circuit has taken into account the presence of both magnets and rotor cage.

The experimental results include no-load and load tests carried out at different voltages and frequencies. The results show a significant performance improvement of the SPLSPMM in comparison to the classical SPIM. The maximum efficiency of the SPLSPMM is higher than 70%, while the efficiency of the SPIM is not higher than 30%.

Nomenclature

α	stator reference angular coordinate
N	number of turns
ω	grid pulsation
φ	angle between the stator and rotor reference
p	number of pole pairs
Kw	winding factor
μ_0	vacuum magnetic permeability
δ	air-gap width
Bpd	direct field
Bpi	reverse field
Ifs	direct component of the stator currents
Ifr	direct component of the rotor currents
Ibs	reverse component of the stator currents
Ibr	reverse component of the rotor currents
BM	residual magnet induction
β	initial angle in rotor reference
ωr	rated motor speed
ρ	stator-to-rotor winding turns ratio
φ	flux linkage
θ	rotor mechanical angle

Author details

Damiano D'Aguanno[1], Fabrizio Marignetti[1]* and Francesco Faginoli[2]

*Address all correspondence to: marignetti@unicas.it

1 Department of Electrical and Information Engineering, University of Cassino and South Lazio, Italy

2 Faber Spa, AN, Italy

References

[1] Miller TJE. Single-phase permanent-magnet motor analysis. IEEE Transaction On Industry Applications. May 1985;**IA-21**(4):651-658

[2] Zelik NG, Dogru UE, Ergene LT. Comparison study of drive motors for cooker hood applications. In: 2014 16th International Power Electronics and Motion Control Conference and Exposition; Sep. 2014. pp. 1252-1258

[3] Varga J, Basic D. Analysis of the characteristics of single phase shaded pole induction motor with two short-circuited auxiliary phases. IEEE Transactions on Energy Conversion. Dec. 1997;**12**(4):269-274

[4] Mansour Ojaghi SD. Analytic model for performance study and computer-aided design of single-phase shaded-pole induction motors. IEEE Transactions on Energy Conversion. Dec. 2016;**32**:649-657. DOI: 10.1109/TEC.2016.2645641

[5] Pessina G, Morra E. Optimization and design of the shaded pole single phase asynchronous motor. In: 2008 IEEE Power and Energy Society General Meeting—Conversion and Delivery of Electrical Energy in the 21st Century. July 2008. pp. 1-4

[6] Fang L, Lee BH, Hong J-P, Nam H. Rotor saliency improved structural design for cost reduction in single-phase line-start permanent magnet motor. In: Energy Conversion Congress and Exposition, 2009. ECCE 2009; IEEE. Sep. 2009. pp. 139-146

[7] Takegami T, Hasegawa M, Tsuboi K, Hirotsuka I, Nakamura M. Basic characteristics of a single-phase line-start permanent magnet synchronous motor. In: 2011 International Conference on Electrical Machines and Systems (ICEMS); Aug. 2011

[8] Shamlou S, Mirsalim M. Design, optimisation, analysis and experimental verification of a new line-start permanent magnet synchronous shaded-pole motor. IET Electric Power Applications. Jan. 2013;**7**(1):16, 26

[9] Zhou J, Tseng K-J. Performance analysis of single-phase line-start permanent-magnet synchronous motor. IEEE Transactions on Energy Conversion. Dec. 2002;**17**(4):453-462

[10] Honsinger VB. Permanent magnet machines: Asychronous operation. IEEE Transactions on Power Apparatus and Systems. Jul. 1980;**PAS-99**(0018-9510):1503-1509

[11] Miller TJE. Synchronization of line-start permanent-magnet ac motors. IEEE Power Engineering Review. Jul. 1984;**PER-4**(0272-1724):57-58

[12] Nam H, Jung SK, Kang GH, Hong JP, Jung TU, Baek SM. Design of pole-change single-phase induction motor for household appli- ances. IEEE Transactions on Industry Applications. May 2004;**40**(7989338):780-788

[13] Lee B-H, Hong J-P, Lee J-H. Optimum design criteria for maximum torque and efficiency of a line-start permanent-magnet motor using response surface methodology and finite element method. IEEE Transactions on Magnetics. Jan. 2012;**48**(12487177):863-866

[14] Popescu M, Miller TJE, McGilp M, Strappazzon G, Trivillin N, Santarossa R. Line-start permanent-magnet motor: Single-phase starting performance analysis. IEEE Transactions on Industry Applications. July 2003;**39**(7709854):1021-1030

[15] Behbahanifard H, Sadoughi A. Line start permanent magnet synchronous motor performance and design; a review. Journal of World's Electrical Engineering and Technology. 2015; **2322**:5114

[16] Sarac V, Atanasova-Pacemska T. Simulation model for prediction of transient performance characteristics of single-phase shaded pole motor. Journal of Electrical Engineering. 2016; **67**(4):253-260

[17] Fang L, Lee BH, Hong J-P, Nam H, Ha S-H. Study on the permanent magnet reduction design in single-phase line-start permanent magnet motor for household appliance. In: 2008 International Conference on Electrical Machines and Systems; Oct 2008. pp. 3289-3292

[18] Miller TJE, Popescu M, Cossar C, McGilp M, Strappazzon G, Trivillin N, Santarossa R. Line-start permanent-magnet motor single-phase steady-state performance analysis. IEEE Transactions on Industry Applications. March 2004;**40**(7943119):516-525

[19] Popescu M, Miller TJE, McGilp M, Strappazzon G, Trivillin N, Santarossa R. Asynchronous performance analysis of a single-phase capacitor-start, capacitor-run permanent magnet motor. IEEE Transactions on Energy Conversion. Feb. 2005;**20**(1):142-150

[20] Rahman MA, Zubayer HM, Wang K, Kurihara K, Osheiba AM, Jabbar MA, Hoque MA. Single phase line-start high efficiency interior permanent magnet motors. In: 2011 IEEE International Electric Machines Drives Conference (IEMDC); May 2011. pp. 19-28

[21] Iepure LI, Tutelea L, Boldea I. Fem analysis and control of a tapered airgap single phase PMSM. In: 2008 11th International Conference on Optimization of Electrical and Electronic Equipment; May 2008. pp. 241-248

[22] Marcic T, Stumberger B, Stumberger G, Hadziselimovic M, Virtic P, Dolinar D. Line-starting three-and single-phase interior permanent magnet synchronous motors;direct comparison to induction motors. IEEE Transactions on Magnetics. Nov 2008;**44**(11):4413-4416

[23] Attaianese C, Pizzo AD, Pagano E. Optimization and modelling of single-phase capacitor motors (in Italian) [PhD thesis]

[24] Huang H, Fuchs EF, White JC. Optimization of single-phase induction motor design: The maximum efficiency and minimum cost of an optimal design. IEEE Transactions on Energy Conversion. June 1988;**3**(2):357-366

[25] Miller TJE. Single-phase permanent magnet motor analysis. In IEEE Transactions on Industry Applications. May 1985;**IA-21**(3):651-658

[26] Popescu M, Miller TJE, McGlip MI, Strappazzon G, Trivillin N, Santarossa R. Line start permanent magnet motor: Single-phase starting performance analysis. IEEE Transactions on Industry Applications. Jul./Aug. 2003;**39**(4)

[27] Popescu M, Miller TJE, McGlip MI, Cossar C, Strappazzon G, Trivillin N, Santarossa R. Line start permanent magnet motor: Single-phase steady-state performance analysis. IEEE Transactions on Industry Applications. Mar./Apr. 2004;**40**(2)

[28] Popescu M, Miller TJE, McGlip M, Strappazzon G, Trivillin N, Santarossa R. Asynchronous performance analysis of a single phase capacitor-start, capacitor-run permanent magnet motor. In IEEE Transactions on Energy Conversion. March 2005;**20**(1):142-150

IntechOpen